LBL-14439
Preprint

Lawrence Berkeley Laboratory
UNIVERSITY OF CALIFORNIA

Submitted to Nuclear Instruments and Methods

BEAM ANALYSES SPECTROMETER FOR RELATIVISTIC HEAVY IONS

Walter Schimmerling, T.S. Subramanian,
W. John McDonald, Selig N. Kaplan,
Ahren Sadoff and George Gabor

July 1982

Prepared for the U.S. Department of Energy under Contract DE-AC03-76SF00098

DISCLAIMER

LBL 14439

Beam Analyses Spectrometer for Relativistic Heavy Ions

Walter Schimmerling, T. S. Subramanian,* W. John McDonald,**
Selig N. Kaplan, Ahren Sadoff*** and George Gabor

Lawrence Berkeley Laboratory
University of California
Berkeley, California 94720, USA

* Permanent address: Swedish American Hospital, Rockford, IL 61101, U.S.A.

** Permanent address: Faculty of Science Office, University of Alberta, Edmonton, Alberta, T6G 2JI, Canada

*** Permanent address: Department of Physics, Ithaca College, Ithaca, NY 14850, U.S.A.

Abstract

A versatile spectrometer useful for measuring the mass, charge, energy, fluence and angular distribution of primaries and fragments associated with relativistic heavy ion beams is described. The apparatus is designed to provide accurate physical data for biology experiments and medical therapy planning as a function of depth in tissue. The spectrometer can also be used to measure W, the average energy to produce an ion pair, range energy, dE/dx, and removal cross section data of interest in nuclear physics.

1. Introduction

When beams of heavy ions are used in radiation therapy and biology (1), the character of the beam is altered as the particles travel through tissue. The velocity of the particles is affected by electromagnetic interactions which slow and spread the beam. Fragments are produced through nuclear interactions and these are also affected by passage through subsequent material. The biological effects produced by the beam are sensitive to the kind of fragments present as well as their fluence, charge and velocity. For example, the RBE (relative biological effectiveness) and OER (oxygen enhancement ratio) depend on all of these quantities (2).

The apparatus described here has been developed to provide complete characterization of the relativistic heavy ion beams used for medical therapy and biology experiments at the Lawrence Berkeley Laboratory BEVALAC (1). It consists of a variable thickness absorber, a time-of-flight (TOF) telescope, and a multi-element detector array.

The absorber which has been used is a remotely controllable double Lucite wedge with fixed thickness inserts (3). Thickness was continuously variable from 1.06 gm/cm^2 to 13.7 gm/cm^2 with the configuration used in the present work. As better data on fragmentation are obtained, it is anticipated that other absorbers such as controlled-thickness water columns will also be used.

Scintillation counters, pulse ionization chambers and multiwire proportional chambers are used for beam identification, definition and tracking. The whole spectrometer is mounted on a movable frame to permit measurements on the beam axis and out to approximately 5°, where all but the lightest and slowest fragments have negligibly small cross sections. The

apparatus has been installed at the exit of a spectrometer magnet which is used to provide momentum analysis of the incident beam particles.

Some of the elements of the spectrometer represent state-of-the-art applications of nuclear instrumentation; other elements are of standard design. The combination of all elements results in a unique spectrometer capable of measuring the charge (and, in a restricted range, the mass), the fluence and the angular distributions of the primary beam and fragment particles over the entire range of material covered by the Bragg curve.

2. Spectrometer Requirements

In order to characterize a beam of heavy ions, it is sufficient to know the distribution in mass, A; charge, Z; velocity, v or momentum, p; position, (x,y) and angle, θ for each ion species in the beam. A and Z can be determined by measuring dE/dx, range and velocity. In the present apparatus dE/dx information is obtained over a wide dynamic range by using gas ionization chambers for the slowest particles, a silicon solid state detector telescope, SST, for faster particles (4), and a NaI scintillation detector plus the SST for the fastest ions. In that part of the dynamic range for which the particles stop in the detectors, the residual range can be used in the A,Z determination. For the fastest particles the SST and NaI detectors perform the function of range sampling. In this case Z can be determined but the resolution for determining A is very poor. Table 1 gives the operating regions for these determinations for each type of detector used in the spectrometer.

Velocity measurement is possible with good precision using a channel plate TOF system (5). The time resolution of this system was found to be

120 ps full width at half-maximum, FWHM (52 ps standard deviation) in the present work. When combined with dE/dx and range information, A,Z could be determined over the dynamic range listed in Table 1.

Position and angle distributions need to be known to define the trajectories for the various ion species in the beam to a moderate accuracy. In most cases the small area of the TOF and SST detector system was sufficient to specify the particle trajectory. Additional information was obtained using multiwire proportional chambers, WC, with delay line readout (6) when necessary. The angular precision obtained in this way was 0.1° when the WC information was not used, and 0.05° when it was.

For clear identification of individual particles, it is necessary to distinguish events in which associated multiple fragments are detected together. This was accomplished with the aid of the SST by making use of the difference in dE/dx and range signals observed for such events. The wire chambers also are able to detect spatially separated multiple particle events, but this possibility has not yet been implemented.

Finally, in order to use a spectrometer to determine the way in which an absorber modifies a heavy ion beam, it is essential to have a well defined primary beam incident on the absorber. For this purpose scintillation counters were used to define the trajectory and the intensity of the incident beam. Pile-up rejection circuitry was employed to select single incident ions (Appendix) and an integrating wire chamber (7) was used to monitor the beam profile for each spill of the BEVALAC accelerator. The primary beam was also momentum-analyzed using a magnetic dipole just upstream of the absorber (8).

3. Description of the Spectrometer

The physical apparatus is shown in the diagram, Figure 1, and the photograph (Figure 2). Table 2 lists the materials in the beam and gives the dimensions of the detectors. The incident beam particles are defined by scintillators S_0 and S_1 in coincidence. The $S_0 \cdot S_1$ signal is referred to as "BEAM". S_0 is a 6.35 mm thick Pilot B scintillator viewed with two photomultiplier tubes. The summed pulse height from the two tubes is independent of position and can be used for pile up rejection (cf. Appendix) as well as a start signal for beam time-of-flight monitoring. The latter measurement was used as a check on the beam time. S_1 is a 3.175 mm thick scintillator viewed by a single photomultiplier and provides a stop signal for the beam time-of-flight.

The small scintillator S_2, 1 cm diameter by 3.175 mm thick, was embedded in a 10 cm x 10 cm x 3.175 mm thick light guide to preserve uniform thickness to particles passing through or by the scintillator. It is used to select a small central spot for sampling the beam composition on the downstream side of the absorber. The thick light guide of S_2 produced some Cerenkov light. Therefore a second scintillator A_1, 3.2 mm thick with a 1 cm central hole filled with a 2.9 mm thick black Micarta disk (to provide uniform energy loss across the detector), was helpful in rejecting the Cerenkov signals.

The TOF telescope (5) consists of two 2 mg/cm^2 thick foils (8 μm Kapton with a 0.1 μm thick Au layer) at an angle of 45° to the beam. Each foil is viewed by a set of chevron channel plate electron multipliers that amplify the secondary electron signal from the foil. These TOF detectors labeled CP_1 and CP_2 in Figure 1 are maintained in a vacuum enclosure at a

vacuum of 10^{-6} Torr. Details of this type of detector are discussed in Ref. 5. Figure 3 is a typical TOF histogram, obtained with an incident argon beam of 509 MeV/A after traversing 4.25 g/cm^2 of Lucite. A contribution of beam fragments may be seen at higher velocity. Part of the measured FWHM is due to the intrinsic velocity spread of the degraded beam and the actual time resolution is probably slightly better.

A solid state detector array (4) follows the TOF telescope to provide multiple sampling of dE/dx for traversing particles and residual range for stopping particles. The array consists of 4 silicon position sensitive devices 5 cm diameter by 500 μm thick (9) labeled P_1- P_4, followed by ten 3 mm thick by 2.5 cm diameter silicon detectors labeled D_1 to D_{10}. A 7.62 cm thick by 7.62 cm diameter sodium iodide scintillator ("NaI") has been added to provide additional range information for the particles which are not stopped in the silicon detectors.

Spatial information for particle trajectory definition is provided by several devices. The integrating wire chamber MWC (7) provides a horizontal (x) and vertical (y) projection of the beam cross sectional area for every beam pulse. The multiwire proportional chambers WC1 and WC2 are of the delay-line readout type (6). They provide x and y position information for each particle in contrast to the integrated profile provided by MWC. The wire spacing in WC1 and WC2 is 3 mm, and a better resolution can be obtained by interpolation. The position of the wire chambers was accurately determined using ^{55}Fe and ^{90}Sr sources collimated to 1 msterad and the resolution was verified to be 2-3 mm. The two pairs of position sensitive solid state detectors P_1- P_4 have been used mainly to measure dE/dx, but can also provide precise trajectory locations at the entrance to the

silicon detector array.

The particles emitted into the detector can be separated into three categories. The lightest and most energetic particles will traverse the detector without stopping. Some particles of intermediate energy, and mass close to that of the beam will stop in the detector. Finally, in the Bragg peak region of the unmodified beam and beyond, as well as in a spread-out Bragg peak, some particles will have a residual range too short to be sampled by the solid state detectors.

For penetrating particles, adequate charge resolution is provided by the TOF-SST combination. In order to identify particles in the immediate vicinity of their Bragg peak, it is necessary to have a detector that is sufficiently thin to allow adequate depth resolution. The ionization chambers IC_1 and IC_2 serve this purpose. They are $\sim$20 mg/cm^2 thick, with a 10-cm diameter sensitive area. These chambers are operated in the pulse mode to provide a charge measurement for each event. Ionization chamber IC_1 measures the total charge emerging from the absorber, while IC_2 identifies only the charge of the fragments traversing the TOF telescope. The ionization chambers were operated with propane gas (C_3H_8), A/CH_4 mixtures (93% A, 7% CH_4), and N_2. Propane is desirable for pulse counting since electron mobility is highest in this gas, but the A/CH_4 mixture is comparable (10) and presents less of a safety hazard. Use of different gases allows for a study of the gas characteristics as a function of particle type and energy (11).

The alignment of the spectrometer is accomplished by mounting all components downstream of the absorber on a movable optical bench and then aligning the bench with respect to the beam axis by use of motor drive

mechanisms. Scintillators A_1 and A_2 are used in anticoincidence with S_1 and S_2, respectively, for this purpose. Scintillator A_1 has been described above; scintillator A_2 has a 1.9 cm central hole. During fragmentation measurements the A_1 and A_2 counter signals were recorded but not in a veto mode, since that would discriminate against multiple particle events. Angular distribution measurements are facilitated by use of a remotely controlled motor drive which can vary the angle of the spectrometer from 0° to ± 5° with the angular setting reproducible to ± 0.04°.

4) Electronics

A simplified block diagram of the electronics is shown in Figure 4. A valid event is signalled by a TRIGGER signal at the interrupt register (IR) of the CAMAC crate. TRIGGER is formed from

$$\text{TRIGGER} = \text{BEAM ON} \cdot (\text{FRONT OR PARTICLE}) \cdot \text{GOOD } S_0 \cdot \overline{\text{INHIBIT}}$$

where:

BEAM ON indicates the BEVALAC is at the flat top and extracting beam;

FRONT = BEAM · S_2 = $S_0 \cdot S_1 \cdot S_2$ indicates a particle incident on the absorber has traversed S_2;

PARTICLE = FRONT · S_3 indicates a particle is incident on the SST;

GOOD S_0 indicates that the S_0 signal does not have pile-up;

$\overline{\text{INHIBIT}}$ means the computer is not busy and S_3 has not seen a particle in the preceding 10 μs.

The circuitry used to detect S_0 pile-up is described in detail in the Appendix. FRONT is used in forming the trigger during alignment while PARTICLE is used in data taking.

The CAMAC coincidence register (CR) records the status of all detectors and logic signals for each event. This allows, for example, the A_1, A_2, A_3 detectors to be used as veto cuts in data analysis if desired, but they do not form part of the event trigger.

CAMAC analog-to-digital converters (ADC) and time-to-digital converters (TDC) were used to record the amplitude and time for signals from the detectors as indicated. Most detector and logic signals were fed to CAMAC scalers (SC) as well. The scalers were read once for each beam spill.

A time-to-amplitude converter (TAC), in combimation with a 13-bit spectroscopy ADC, was used to obtain the precise TOF for each event. The range of velocities varies over a factor of 4; with a resolution of 0.1%, this requires that the ADC have at least 12 bits (4096 channels), as well as the appropriate linearity. Available TDC's had only 11 bits of resolution and were not adequate for this application.

Scintillation counters S_0, S_1, S_2, S_3, A_1, A_2, A_3 have high rate bases (12) which include transistor stabilized divider supplies.

The solid state detector electronics system is described in Ref. 13. It consists of a set of low noise amplifiers and a precision pulser system to facilitate calibration.

The rest of the electronics was of standard design.

5. Data Acquisition and Analysis

A schematic diagram of the data flow is shown in Fig. 5. Every beam particle traversing the spectrometer, that satisfied the requirements of the electronic logic, constituted an event. Each event consisted of forty 16-bit words read from the CAMAC units by a PDP/11-34 computer via a microprogrammed branch driver (MBD). Data from those events were acquired during the $\sim$1 sec duration of the heavy ion beam pulse. In the $\sim$4 sec interval between pulses, data accumulated during the pulse but not read were transferred to the computer. These data were the integrating multiwire proportional chambers recording the beam profile and scaler counts. At appropriate intervals "housekeeping" information (e.g. absorber thickness) was also recorded.

The software used for data acquisition and on-line analysis, QDA and MULTI, was developed at Fermilab and modified at LBL. These programs recorded the data on magnetic tape and also provided current information on selected histograms, scaler counts, etc. The recorded data could be played back for off-line analysis subsequent to data taking.

A carefully timed series of pulser signals was used to simulate the beam for calibrations and testing of the detectors. These data were also recorded.

Data were transferred from magnetic tape to disk for off-line analysis, using a program that we developed for this purpose, SIFT. A fairly elaborate record-keeping system is required by the data, which are taken under a broad variety of experimental conditions, and maintaining this system is a further purpose of SIFT. With it, events satisfying a variety of software cuts are selected from the tape records and packed into disk rec-

ords. A detailed label record, consisting of information on the beam particle and energies, the exact configuration of elements in the beam line, the calibration disk files to use for the particular run, the software cuts made, and the assignment of event words to experimental quantities, is created and added to the record, with a minimum of operator intervention. In addition, all the scaler data are accumulated and preserved in the label record. SIFT also records which runs are used to create a combined file, and creates a prescribed disk file specification for the output data. Data can be transferred back to tape or to another disk.

The data processed by SIFT can be used for event-by-event analysis. The analysis program converts the recorded pulse heights and times to energy deposition in the detectors and to velocity in the TOF telescope, using the appropriate calibration factors. It then propagates each particle through the apparatus and identifies the particle by a least squares fit between the calculated and the observed quantities. Biophysical quantities, such as the linear energy transfer (LET), dose, and dose-averaged LET, and their distribution, are calculated for each identified component of the beam.

The identification algorithm is based on the principles described by Greiner (4), and seeks a least squares minimum of the difference between calculated and measured signals for a set of trial A and Z. Fig. 6 shows an average distribution of the resultant chi-squared values for a primary ^{19}Ne beam and secondary oxygen fragments. A very sharp minimum may be seen for neon, whereas a shallow minimum is seen around A = 14 for oxygen in this event, reflecting the fact that the oxygen ions do not stop in the SST, and that an inadequately small fraction of the oxygen range has been

sampled for mass identification.

The results of a Monte Carlo calculation of the expected distribution of signals due to nitrogen in the first silicon detector ("D_1") as a function of the total energy deposited in the SST ("SUM") is shown as a scatter plot in Fig. 7, to illustrate some of the data analysis problems. The incident beam (assumed to be nitrogen) appears as an island (I). Nuclear interactions in the detector appear as a tail depositing less total energy (II). The fragments accompanying the beam, each with its own nuclear interaction tail, appear in region III. Fig. 8 shows similar data for a measured beam stopping in the SST. Fig. 9 shows the total energy loss projection onto the SUM axis, where elements and some isotopes can be clearly distinguished.

The problem of distinguishing fragments present in the beam from fragments produced in the detector and the problem of resolving coincident multiple fragments is alleviated by the additional availability of TOF information and the multiple sampling nature of the SST, where these effects appear as statistically significant deviations in energy loss along the detector stack.

The analysis programs are still being optimized but the capability of the MULTI software is already sufficient to obtain significant results. For this reason, the description of apparatus performance is based on MULTI.

6. Alignment, Calibration and Acceptance

A spectrometer alignment procedure is necessary to ensure that the device is accurately positioned with respect to the center line of the beam.

First, with the absorber removed, the beam is positioned on S_2 using the bending magnet while the ratio (FRONT · $\overline{A}_1$)/BEAM is maximized. A typical result obtained with this procedure is shown in Fig. 10a. The peak of the curve, at 17.5%, represents the ratio of the area of S_2 to the effective beam area. The small size of the source-defining scintillator also results in a momentum bite, $\Delta p/p$, of 0.8% comparable to the intrinsic momentum dispersion of the beam. The magnet was calibrated using wire orbiting (8) and its results agreed with those obtained using the TOF telescope. The vertical alignment is adjusted with the aid of a motor-driven screw which sets the height of the spectrometer at the upstream end to further optimize (FRONT · $\overline{A}_1$)/BEAM.

The downstream alignment of the spectrometer involved a calibration of the angular setting to establish $\theta = 0°$. This was done by observing (PARTICLE · $\overline{A}_2$)/(FRONT · $\overline{A}_1$) while the spectrometer angle was adjusted using its remotely controlled drive. A typical result is shown in Fig. 10b. The area under this beam profile is only 70% of BEAM, reflecting the presence of the 2.5-cm diameter collimator.

The observed angular spread results from divergence of the beam (0.5°) and the finite angular acceptance of the spectrometer (0.1°). The beam divergence, and consequently the acceptance, will vary as a function of absorber thickness. Fig. 11 illustrates this effect as manifested in the ratio PARTICLE/FRONT (without anticoincidences) obtained from scaler ratios for different values of the Lucite absorber thickness (data points) and a slightly different beam spot than the one shown in Fig. 10b. The problem of evaluating the fraction of counts detected by S_3 in the presence of multiple scattering was analyzed by Sternheimer (14), who gives formulae ade-

quate for numerical integration. The effect of energy loss in a thick absorber was already considered by Molière (15) who proved that, with reasonable assumptions, the shape of the multiple scattering distribution remains the same if the square of the mean spatial angle is scaled by $1/(1 - x/R)$, where x is the absorber thickness and R is the range of the incident beam. A calculation based on these prescriptions is shown as the broken line in Fig. 11, normalized to the minimum absorber thickness point. The normalization factor, $\sim$62%, is in good agreement with the fraction of beam transmitted by the collimator.

The ratio of Fig. 11 reflects mainly the effect of multiple scattering by the primary neon ions. To obtain a similar acceptance curve for individual fragments, the width of the angular distribution as given for projectile fragmentation e.g. by Goldhaber (16) must be added in quadrature. Since this width is comparable to that of multiple scattering, the acceptance will be reduced by a further factor of $\sim$2 for projectile fragments. This is further illustrated in Fig. 12, showing charge spectra obtained at 0°, 0.4° and 0.8°, for a 3.4 g/cm^2 Al absorber. The spectra show the shift in relative abundance as the angle is increased, due to the combination of nuclear and multiple Coulomb scattering. The Al absorber is not thick enough to introduce observable fragment depletion, but this effect becomes important for thicker absorbers.

The angular resolution of the detector is small enough to be used for angular distribution measurements such as are shown in Fig. 12. When better angular definition is needed the wire chambers, WC, are used; their instrumental angular definition is much smaller than the beam divergence.

The absorber parameters are listed in Table 2. The fixed inserts were

uniform to the level of a few parts in 10^5 and the wedge thickness was reproducible to 0.013 gm/cm^2.

Time dispersions for the TAC and TDC's were obtained using an ORTEC precision time calibrator. The TAC-ADC combination used for the time-of-flight measurement was typically operated with a time dispersion of 7 ps/ch and a range of 50 ns. The observed spread in time for the primary beam without absorber was 52 ps. Nonlinearity was on the order of ± 5 channels or ± 35 ps over the time range used.

The SST system was calibrated by adjusting each detector's amplifier to give the same gain as measured with the precision pulsing system (13). The calibration was then verified using a 670 MeV/A ^{20}Ne beam. The results are given in Table 3.

Calibration of the ionization chambers is described elsewhere (11).

7. Acknowledgments

This work was supported by the United States Department of Energy under contract number DE-AC03-76SF00098 and by the Public Health Service of the United States Department of Health and Human Services under grant number ROI CA23247, awarded by the National Cancer Institute. A preliminary data acquisition system and the philosophy that keeps the data in order was developed by W. F. Steele. E. Harvey adapted MULTI/QDA for our use and provided valuable continuing assistance in its implementation. D. Meier designed and built the mechanical assembly, gas flow systems and control electronics. D. Landis designed the silicon detector electronics and provided valuable advice throughout. We thank D. Greiner for the loan of the silicon detectors, J. A. Simpson for the loan of the position-sensitive detectors, and V. Perez-Mendez for the loan of the wire chambers. H.

Crawford has helped with beam line setup and many stimulating conversations. J. W. Kast and D. Ortendahl contributed to preliminary versions of this work. The help of F. Bieser, I. Flores and M. Strathman is gratefully acknowledged. This work would not have possible without the dedicated efforts of R. Force, J. Howard, F. Lothrop and the BEVALAC staff. One of us (WS) also wishes to express his gratitude for the continuing support and encouragement received from E. Alpen.

References

(1) Biological and Medical Research with Accelerated Heavy Ions at the BEVALAC, ed., M. D. Pirrucello and C. A. Tobias (Lawrence Berkeley Laboratory Report LBL-11220, 1980).

J. R. Castro and J. M. Quivey, Int. J. Oncol. Biol. Phys. 3 (1977) 127.

(2) E. A. Blakeley, C. A. Tobias, T. C. H. Yang, K. C. Smith and J. T. Lyman, Radiat. Res. 80 (1979) 122.

(3) W. Schimmerling, J. Alonso, R. Morgado, C. A. Tobias, H. Grunder, F. T. Upham, A. Windsor, R. A. Armer, T. C. H. Yang and J. Gunn, IEEE Trans. Nucl. Sci. NS-24 (1977) 1049.

(4) D. E. Greiner, Nucl. Inst. and Meth. 103 (1972) 291.

(5) G. Gabor, W. Schimmerling, D. E. Greiner, F. Bieser and P. Lindstrom, Nucl. Inst. and Meth. 130 (1975) 65.

(6) P. Lecompte, V. Perez-Mendez and G. Stoker, Nucl. Inst. and Meth. 153 (1978) 543.

(7) J. Cuperus and R. Morgado, IEEE Trans. Nucl. Sci. NS-22 (1975) 1561.

(8) H. Crawford, The Beam 40 Facility, LBL internal report (1981).

(9) J. E. Lamport, G. M. Mason, M. A. Perkins and A. J. Tuzzolino, Nucl. Inst. and Meth. 134 (1976) 71. (Detectors fabricated by A. J. Tuzzolino.)

(10) J. W. Epstein, J. I. Fernandez, M. H. Israel, J. Klarmann and R. A. Mewaldt, Nucl. Inst. and Meth. 95 (1971) 77.

(11) W. Schimmerling, S. Kaplan, T. S. Subramanian, W. J. McDonald and E. Alpen, Proc. Int. Conf. on Microdosimetry (Julich, Germany, September 1982. To be published.)

(12) C. R. Kerns, IEEE Trans. Nucl. Sci. NS-24 (1977) 353.

(13) D. A. Landis, S. L. Lu and W. Schimmerling, Lawrence Berkeley Laboratory Report LBL-14156 (1982).

(14) R. M. Sternheimer, Rev. Sci. Instr. 25 (1954) 1070.

(15) G. Molière, Z. Naturforsch. 3a (1948) 78.

(16) A. S. Goldhaber, Phys. Lett. 53B (1974) 306.

List of Tables

Table 1

Spectrometer Specifications

Parameter	Ion Species	Range	Precision	
Velocity (v)	All	$v > 0.0642$ m/ns	$\frac{\Delta\beta}{\beta} = \frac{\Delta t}{t} = \frac{52}{t}$ ps $\beta = .25$ to 1	
Angle	All	0° to 5°	0.04°	
A	≥ 6	stopping particles	$\frac{\Delta m}{m} \leq 10\%$	
$\not{Z}$	≥ 3 ≥ 1		$\not{Z} \leq 0.2$	SST only NaI included

Table 2

Material in Beam [a]

Name	Dimensions (cm)	$\rho\Delta x$ (g/cm^2)	Material
So	20 x 20 x 0.6	0.703	Pilot B
MWC	5 (diam) x 2	0.050	[Water Equivalent]
S_1	7.5 x 7.5 x 0.3	0.359	Pilot F
Fixed Absorber Inserts	10 x 10 x(1.27 or 2.54)	1.454 - 8.912	Polymethylmethacrylate
Wedge	5 x 7.5 Δx(variable x)	$1.307 \times 10^{-3}\Delta x + 1.0618$	Polymethylmethacrylate
Extra Absorbers	Various	Various	Various
A_1	10 x 10 x 0.3	0.359	Pilot F
S_2	1 cm diam x 0.3	0.359	Pilot F
WC_2	28 x 53 x 2	0.050	[Water Equivalent]
IC_1	10 cm diam x 5.7	0.014	[Water Equivalent]
TOF Telescope	2 cm diam x 339	0.003	[Water Equivalent]
TOF Windows	20 cm diam x 0.03	0.070	Mylar
IC_2	10 cm diam x 5.7	0.014	[Water Equivalent]
WC_3	53 x 28 x 2	0.050	[Water Equivalent]
S_3	1.9 cm diam x 0.3	0.359	Pilot B
P_1-P_4	5.08 cm diam x 0.23	0.535	Silicon
D_1- D_{10}	2.54 cm diam x 3.2	7.685	Silicon
NaI	7.5 cm diam x 7.5	27.97	NaI

[a] Air paths not included

Table 3

Solid State Detector Resolution

Number	σ MeV	E MeV	σ/E %	$\sigma/\sqrt{E}$
1	3.46	146	2.4	.29
2	3.51	153	2.3	.28
3	3.27	150	2.2	.27
4	3.43	150	2.3	.28
5	3.30	147	2.2	.27
6	3.42	152	2.3	.28
7	3.82	153	2.5	.31
8	3.58	155	2.3	.29
9	3.75	154	2.4	.30
10	3.82	155	2.5	.31

Figure Captions

Fig. 1 Horizontal cross section of spectrometer. "SCALE" indicates a calibrated rail showing displacement along an arc of the upstream bending magnet used for momentum analysis of the incident beam. The apparatus pivots about an axis perpendicular to the beam line at the wedge exit; the rotation radius to wheels placed under CP_2 is shown as r = 3.75 m (note that the vertical and horizontal scales are different in the figure). A third available location for a TOF detector is shown as (CP_3), but was not used. The other elements are described in the text.

Fig. 2 Top: photograph of the installed apparatus. Bottom, left: close-up view of downstream end of spectrometer. Bottom, right: close-up view of upstream end.

Fig. 3 Time-of-flight spectrum of argon ions, degraded to 509 MeV/A. Secondary fragments produced in the degrader appear at higher velocity (the time scale to the ADC channels increases from right to left).

Fig. 4 Schematic diagram of electronic logic.

Fig. 5 Schematic diagram of data flow.

Fig. 6 Example of chi-squared for particle identification for primary neon-19 and a penetrating, secondary oxygen fragment.

Fig. 7 Simulated scatter plot of energy loss in first silicon detector vs. total energy loss in detector stack, for incident nitrogen. Region I corresponds to primary nitrogen; region II corresponds to primary nitrogen suffering nuclear interactions in the stack; region III corresponds to secondary fragments, produced in an upstream energy degrader. The nuclear interactions suffered in the stack by these fragments are also shown.

Fig. 8 Scatter plot obtained with a neon beam stopping in the silicon detector stack. Note the similarities to the simulated data in Fig. 7.

Fig. 9 Histogram of the data in Fig. 8, projected onto the SUM axis.

Fig. 10 a) Ratio of electronic logic signals defining the upstream apparatus center as a function of momentum calculated from bending magnet used for alignment. The momentum bite (FWHM) defined by the detector is 0.8%.

b) Ratio of electronic signals defining the apparatus alignment as a function of displacement perpendicular to the beam axis. The full width at half-maximum is 3 cm for a beam spot diameter of 2 cm.

Fig. 11 Ratio of PARTICLE/FRONT as a function of absorber thickness, related to detector acceptance. The open squares are data points obtained for neon ions incident on the absorber at 660 MeV/A (range $\sim$ 35 g/cm^2). The dashed curve is the effect of multiple scattering, normalized to the minimum thickness point. The normalization is in good agreement with collimator transmission.

Fig. 12 Charge spectra obtained at 0°, 0.4°, and 0.8° for 670 MeV/A neon beam, incident on a 1-cm thick aluminum target.

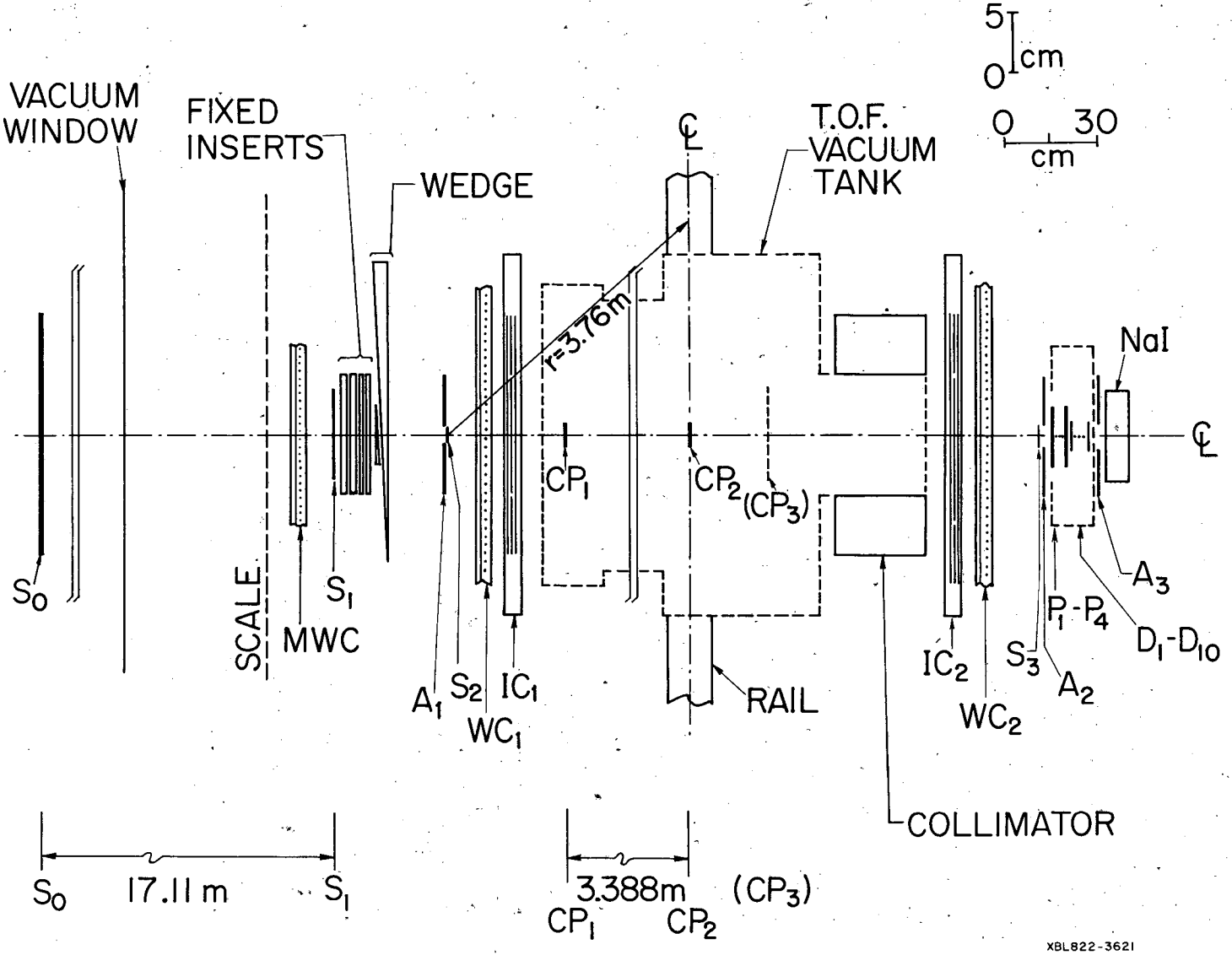
VACUUM WINDOW
FIXED INSERTS
WEDGE
T.O.F. VACUUM TANK
5 cm 0
0 30 cm
r=3.76m
NaI
S_0
SCALE
MWC
S_1
A_1
S_2
WC_1
IC_1
CP_1
CP_2 (CP_3)
RAIL
COLLIMATOR
IC_2
WC_2
S_3
A_2
P_1-P_4
A_3
D_1-D_{10}
S_0 17.11 m S_1
3.388m (CP_3)
CP_1 CP_2
XBL822-3621

Fig. 1

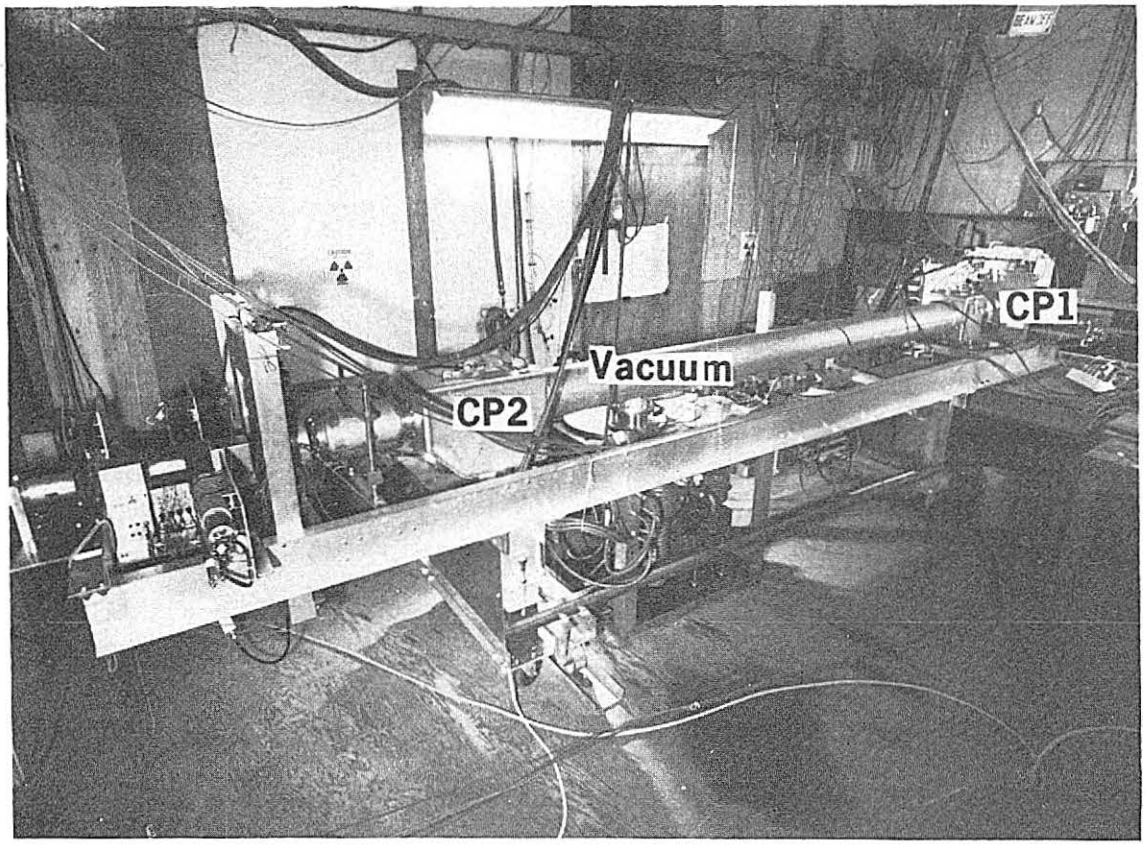

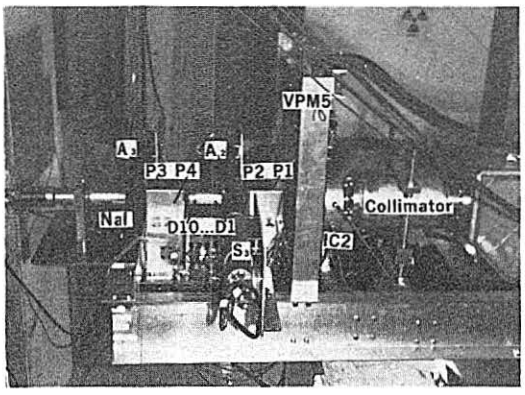

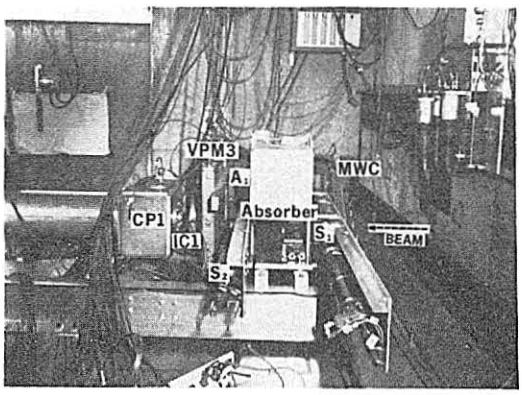

XBB 803-3439A

Fig. 2

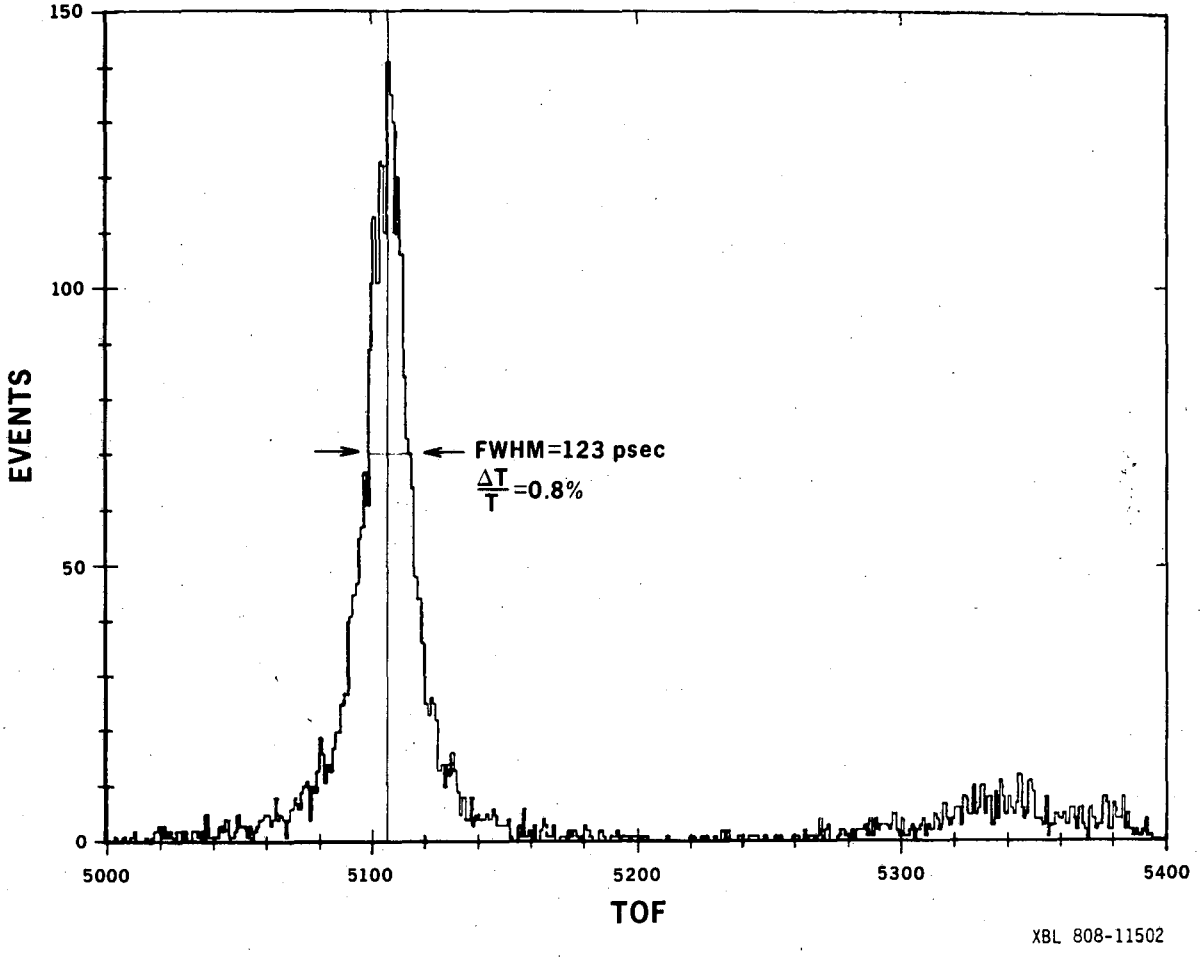
150
100
50
0
EVENTS
FWHM=123 psec
ΔT/T=0.8%
5000
5100
5200
5300
5400
TOF
XBL 808-11502

Fig. 3

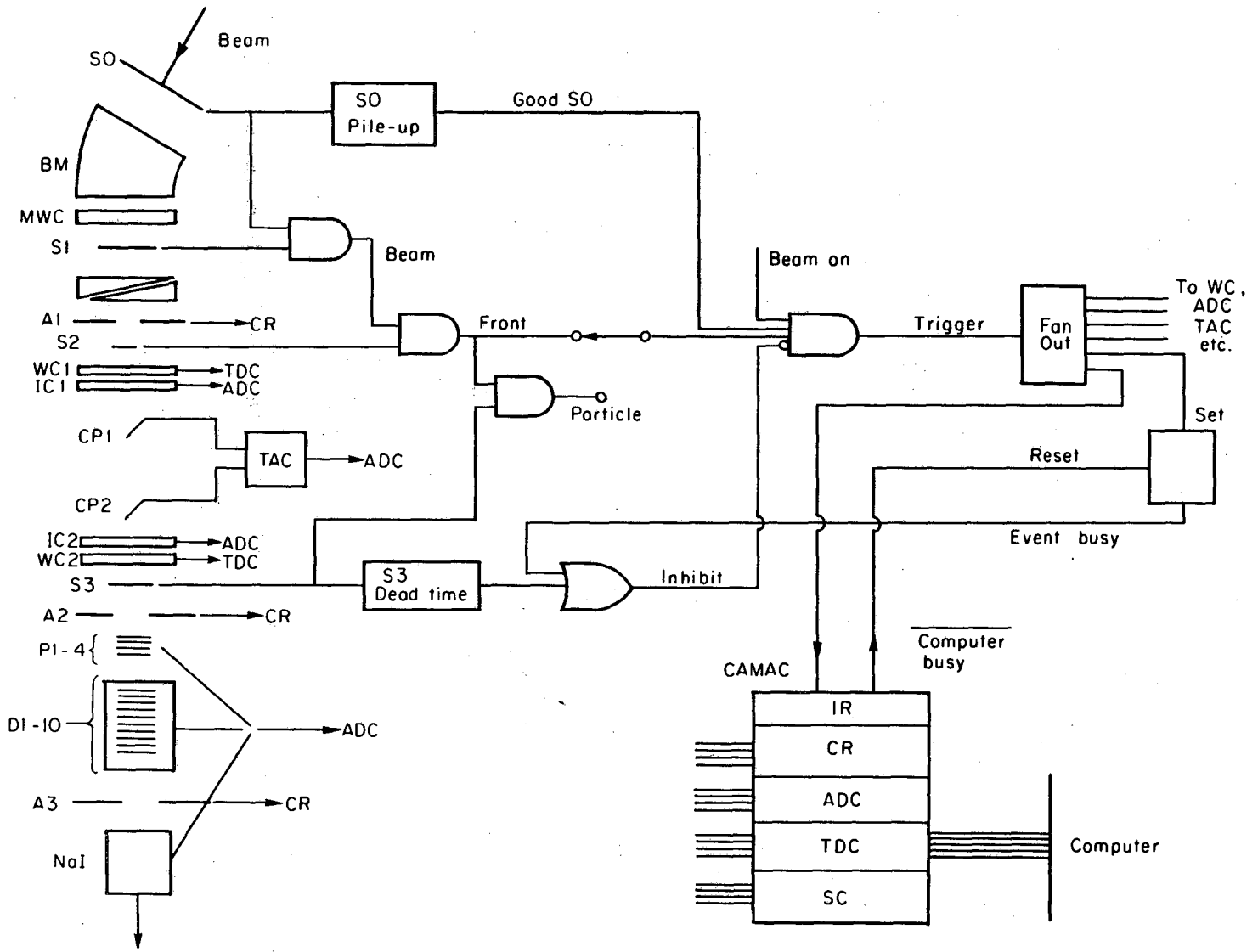

Fig. 4

XBL824-3785

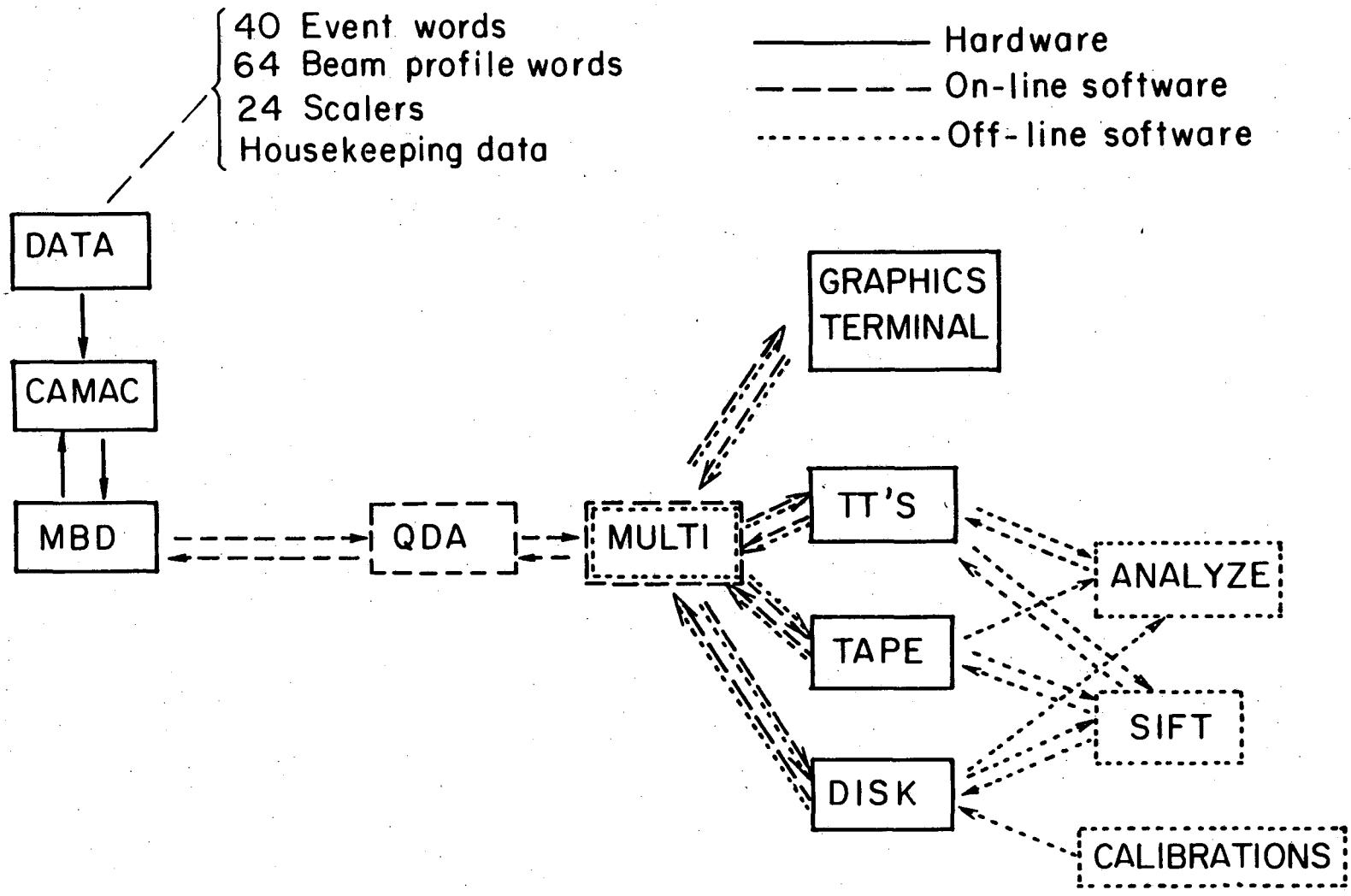

Fig. 5

XBL815-3838

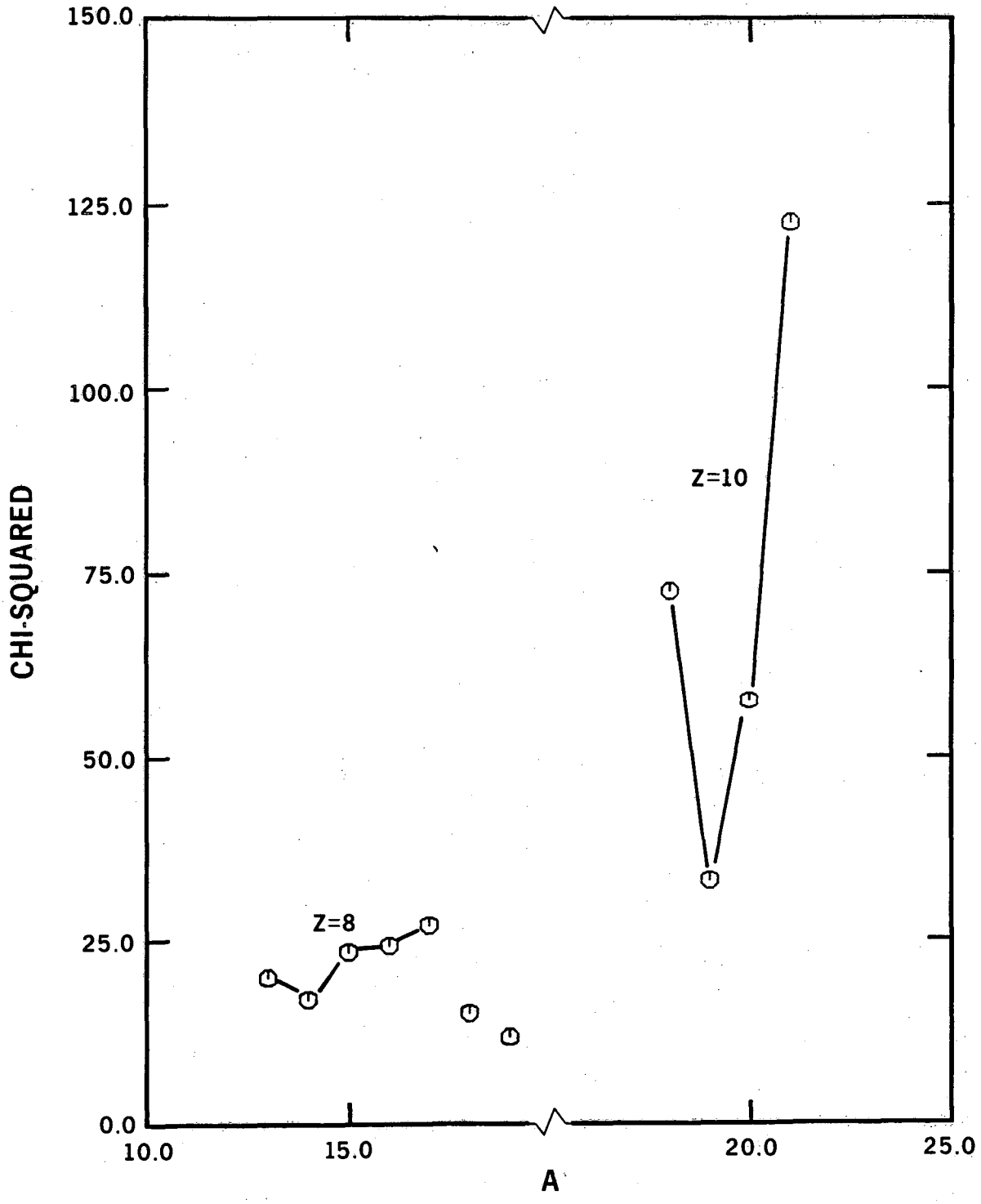

XBL 808-11503

Fig. 6

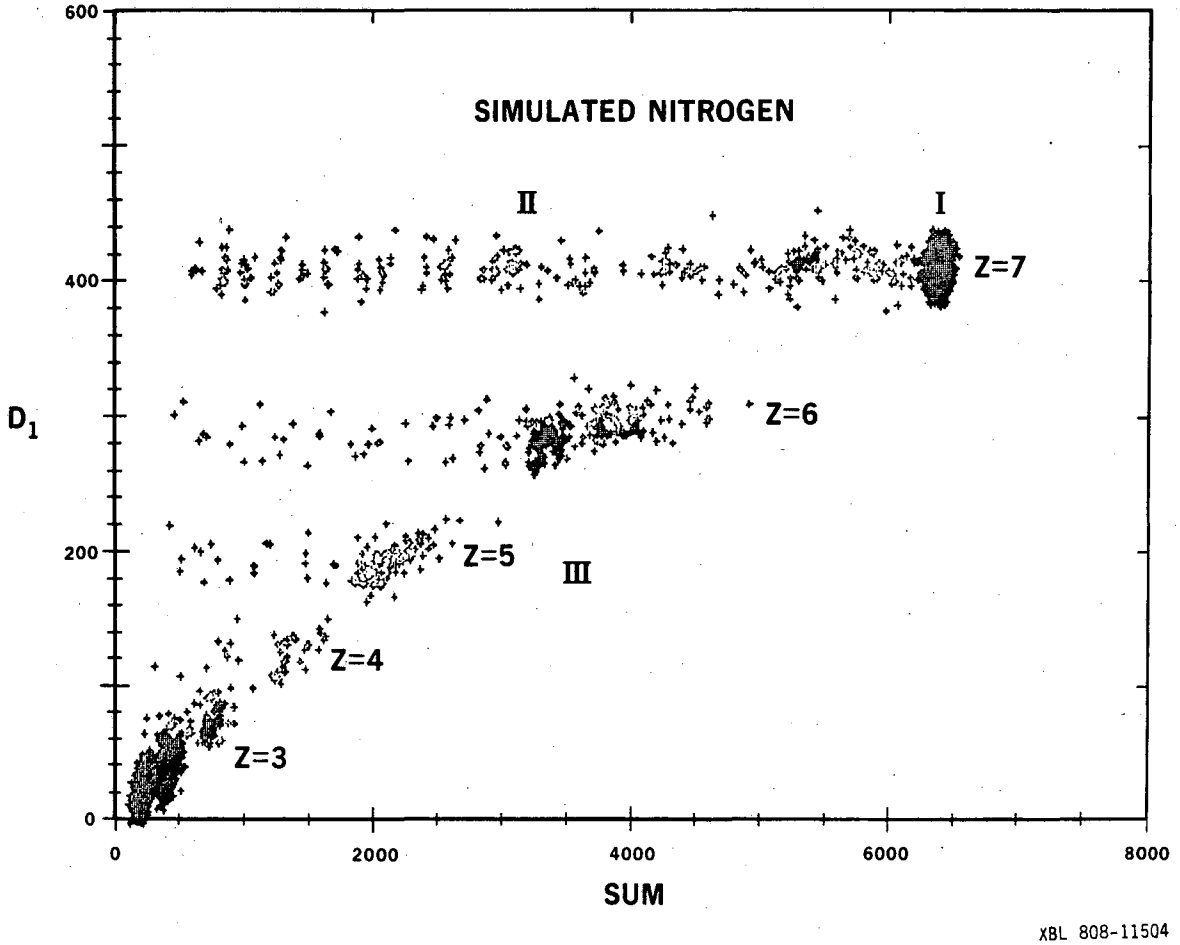
SIMULATED NITROGEN
II
I
Z=7
Z=6
Z=5
III
Z=4
Z=3
D1
SUM
600
400
200
0
0
2000
4000
6000
8000
XBL 808-11504

Fig.7

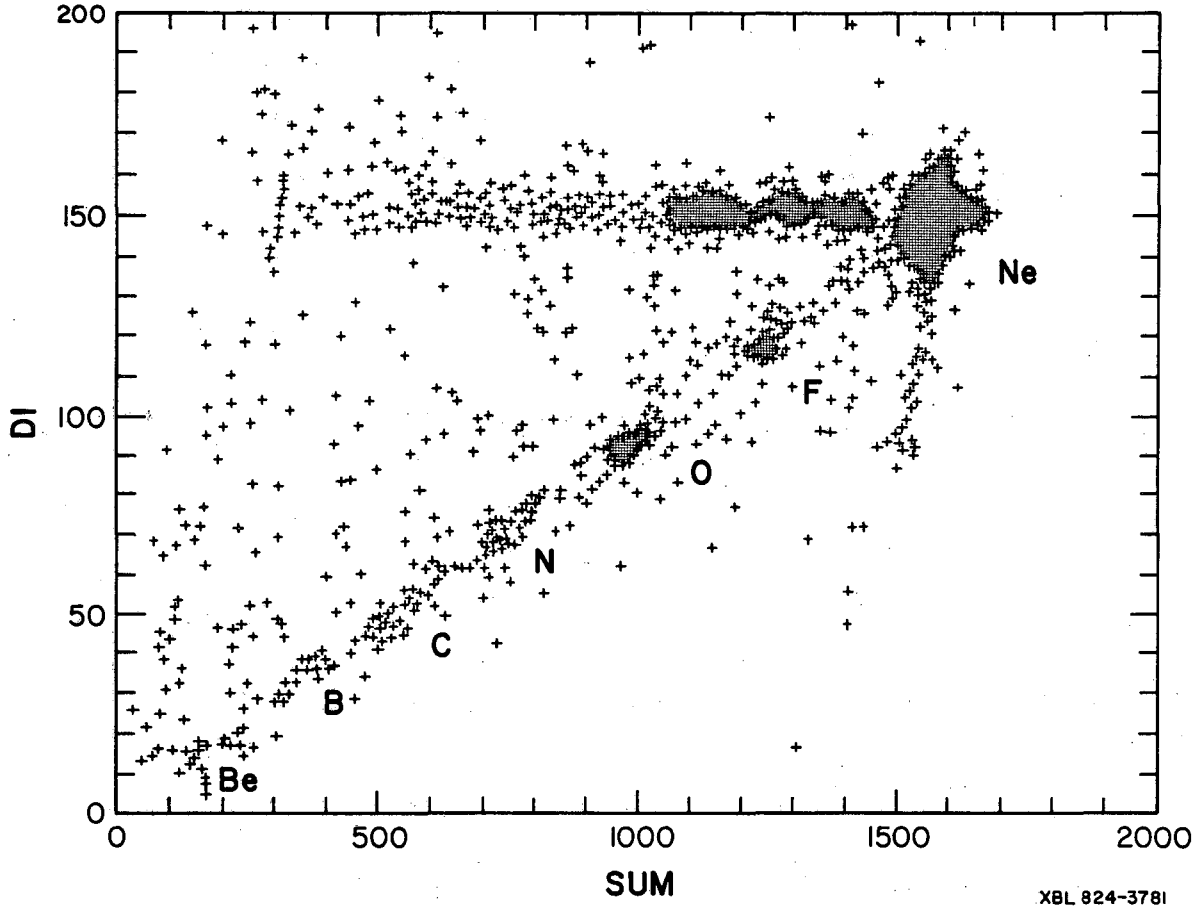
200
150
100
50
0
DI
0
500
1000
1500
2000
SUM
Be
B
C
N
O
F
Ne
XBL 824-3781

Fig.8

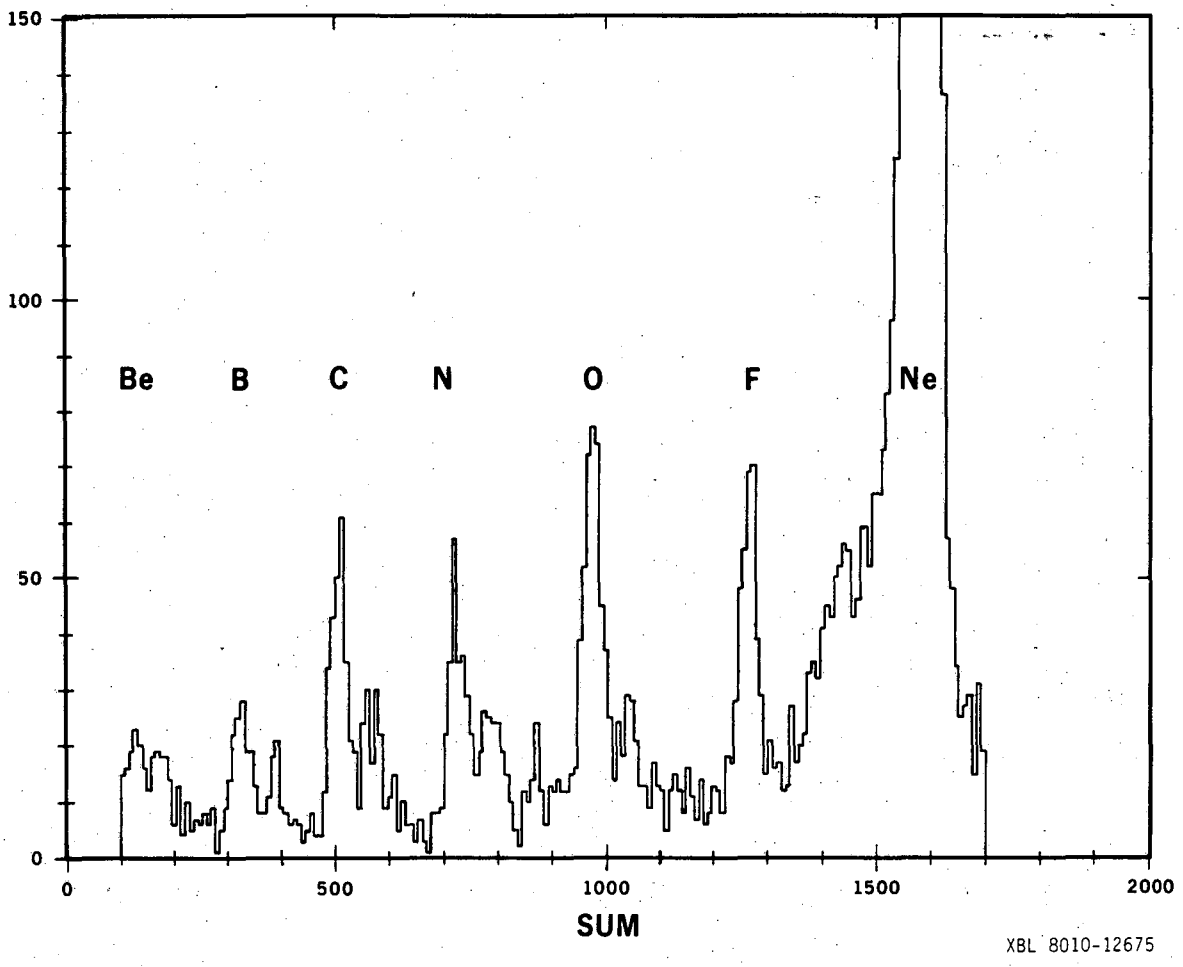

Fig. 9

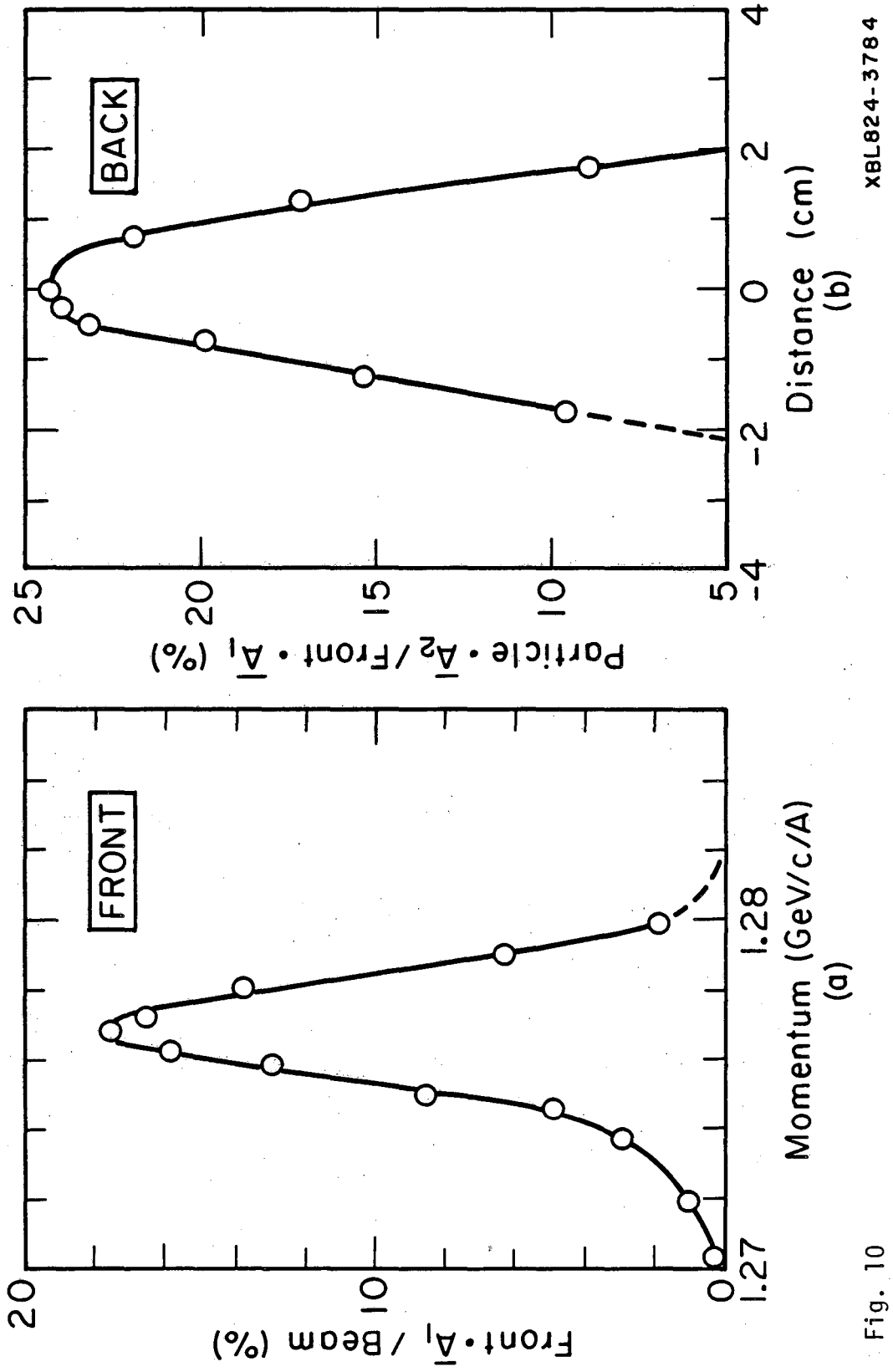
FRONT
Front • $\bar{A}_1$ / Beam (%)
20
10
0
1.27
1.28
Momentum (GeV/c/A)
(a)
BACK
Particle • $\bar{A}_2$ / Front • $\bar{A}_1$ (%)
25
20
15
10
5
-4
-2
0
2
4
Distance (cm)
(b)
XBL824-3784

Fig. 10

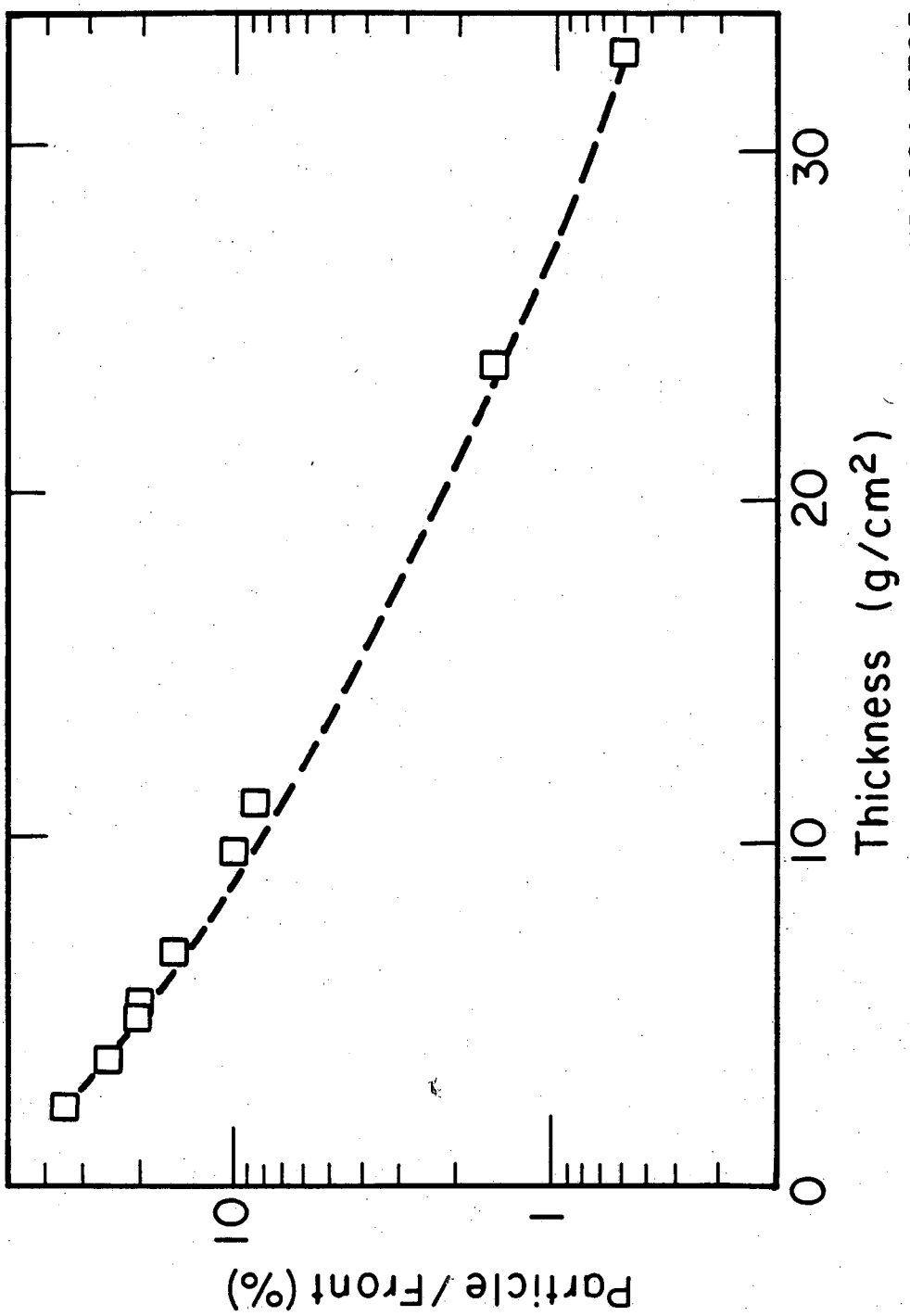

Fig. 11

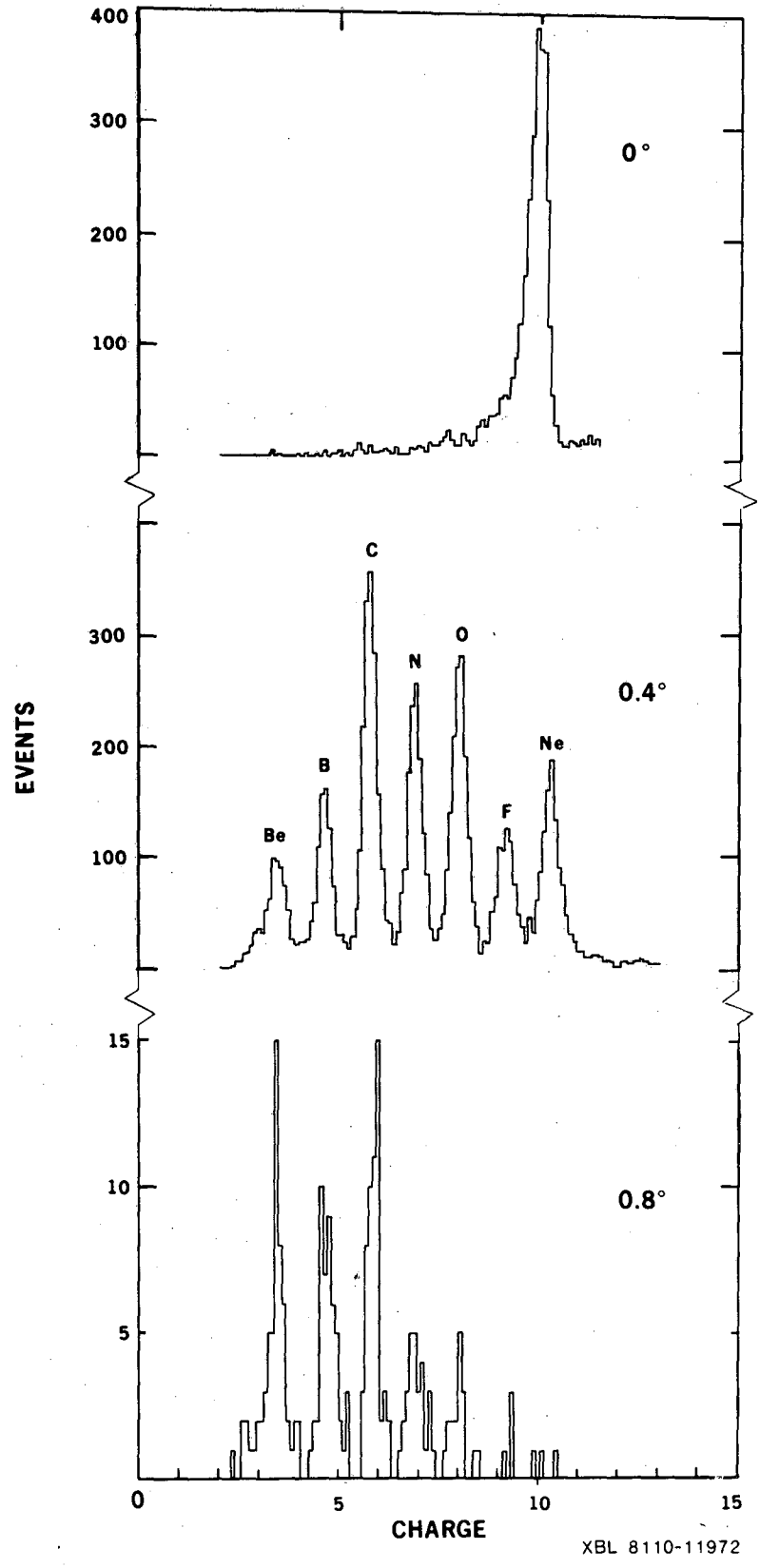
400
300
200
100
0°
300
200
100
C
N
O
0.4°
B
Be
F
Ne
EVENTS
15
10
5
0.8°
0
5
10
15
CHARGE
XBL 8110-11972

Fig.12

Appendix

Pileup Rejection Scheme

A block diagram of the pileup rejection unit is shown in the top of Fig. A-1. This pileup rejector has true zero dead time, i.e. infinite time resolution. Zero dead time is achieved by using a dual coincidence measuring circuit. The first is an analog system which takes advantage of the moderate energy resolution that the plastic scintillator has with heavy ions and a mono-energetic beam. Integrating the charge deposited during an inspection time and comparing it against a threshold equivalent to one and a half times the charge produced by a single particle in effect give infinite coincident time resolution. The second circuit is a standard digital coincidence comparator which fires if a second particle passes through the scintillator during the balance of the inspection time.

The detailed circuit works in the following fashion (cf. timing diagram at bottom of Fig. A-1): the analog and digital inputs must be set to arrive at the same time. The delay D1 insures that the sampling bridge is gated open when the analog signal arrives at the integrator. The integrator is open for approximately 30 ns. The charge comparator following the integrator is set to reject pulses greater than 200 mV into 50Ω x 10 ns. It is reset when the sampling bridge closes. The sampling of the analog signal by the pileup rejection module is necessary because even so-called dead-timeless circuits have dead times of 4 ns upward.

The digital input triggers an inspection one-shot that produces a pulse width equal to the digital pileup inspection time (30 - 400 ns), starting about 10 ns after the digital input (the width of the digital pulse). This

delay insures that the digital input and the one-shot pulse are never in coincidence. If no further digital inputs arrive while the one-shot is on, there is no signal output at the coincidence output (6). If there is a second (or more) digital input during the inspection time, the one-shot is updated, the next digital signal is in coincidence with the one-shot output, and a signal is fed into the OR, setting the pileup rejection veto. If the second input arrived too early to update the one-shot, its analog input will overlap with that of the first signal, producing a signal at the output of the charge comparator, satisfying the OR logic, and setting the pileup reject veto.

The digital input is tested for coincidence with the pileup reject signal after a delay equal to the inspection time, provided by a cable of suitable length. A delay cable is used to permit good timing resolution on the validated pulse. The duration of the inspection time one-shot is adjusted to match the cable delay.

After the inspection time, the pileup reject veto is reset following a delay of approximately 10 ns. Thus, an output is produced only if a time interval greater than the (updated) inspection time has elapsed between two signals. If the interval is smaller, neither signal will result in a valid out. This is equivalent to inspecting the time prior to, as well as the time following the signal for occurrence of pileup.

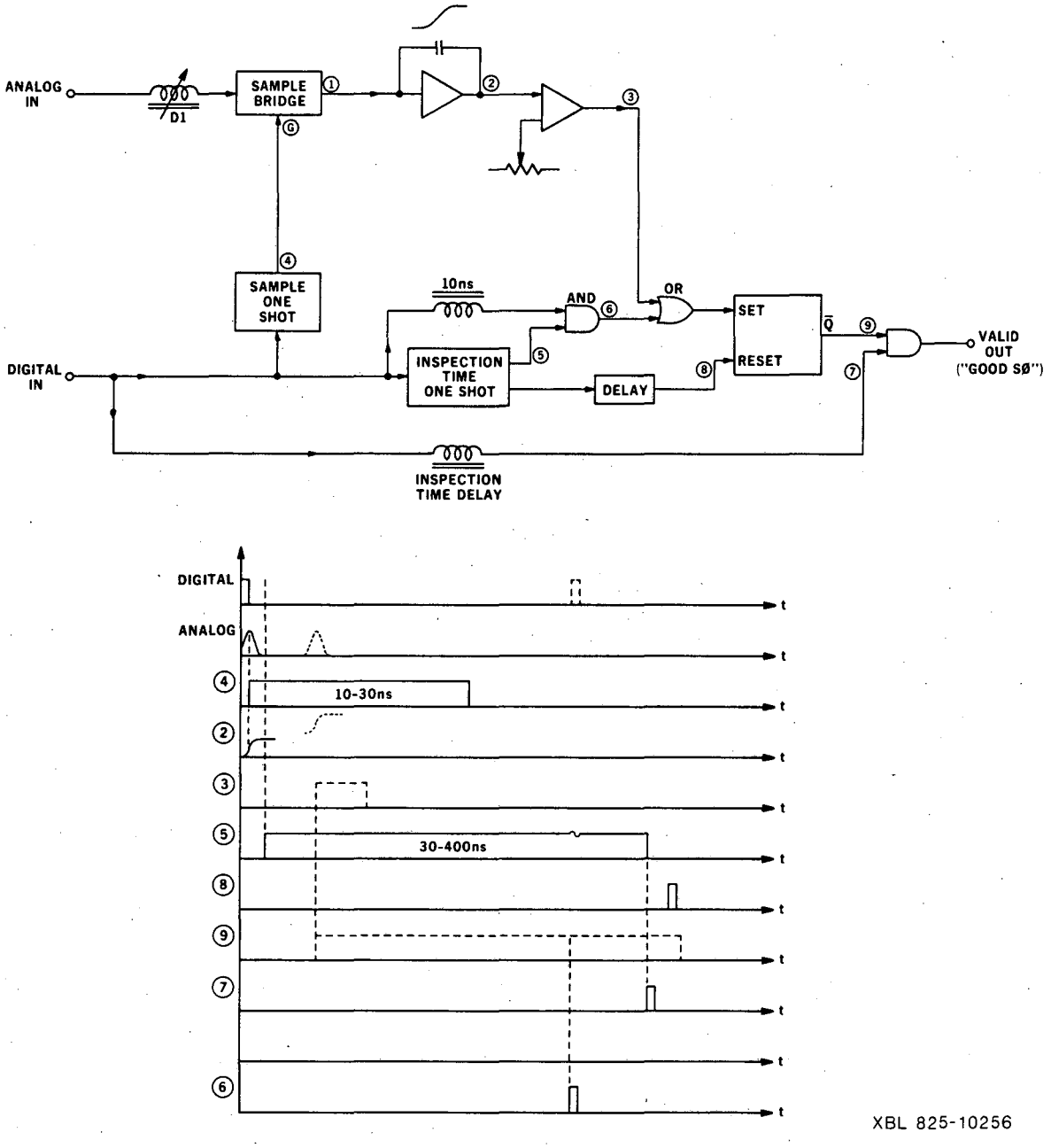
ANALOG IN
D1
SAMPLE BRIDGE
SAMPLE ONE SHOT
10ns
AND
OR
SET
RESET
Q̄
VALID OUT ("GOOD SØ")
DIGITAL IN
INSPECTION TIME ONE SHOT
DELAY
INSPECTION TIME DELAY
DIGITAL
ANALOG
10-30ns
30-400ns
t
XBL 825-10256

Fig. A-1

TECHNICAL INFORMATION DEPARTMENT
LAWRENCE BERKELEY LABORATORY
UNIVERSITY OF CALIFORNIA
BERKELEY, CALIFORNIA 94720